Published in final edited form as:
Dev Biol. 2012 July 1; 367(1): 1–14. doi:10.1016/j.ydbio.2012.04.012.

Interaction of Wnt3a, Msgn1 and Tbx6 in neural versus paraxial mesoderm lineage commitment and paraxial mesoderm differentiation in the mouse embryo

Sonja Nowotschin[1], **Anna Ferrer-Vaquer**[1], **Daniel Concepcion**[2], **Virginia E. Papaioannou**[2], and **Anna-Katerina Hadjantonakis**[1,*]

[1]Developmental Biology Program, Sloan-Kettering Institute, New York, NY 10065, USA

[2]Department of Genetics and Development, Columbia University Medical Center, New York, NY 10032, USA

Abstract

Paraxial mesoderm is the tissue which gives rise to the skeletal muscles and vertebral column of the body. A gene regulatory network operating in the formation of paraxial mesoderm has been described. This network hinges on three key factors, Wnt3a, Msgn1 and Tbx6, each of which is critical for paraxial mesoderm formation, since absence of any one of these factors results in complete absence of posterior somites. In this study we determined and compared the spatial and temporal patterns of expression of *Wnt3a*, *Msgn1* and *Tbx6* at a time when paraxial mesoderm is being formed. Then, we performed a comparative characterization of mutants in *Wnt3a*, *Msgn1* and *Tbx6*. To determine the epistatic relationship between these three genes, and begin to decipher the complex interplay between them, we analyzed double mutant embryos and compared their phenotypes to the single mutants. Through the analysis of molecular markers in mutants, our data support the bipotential nature of the progenitor cells for paraxial mesoderm and establish regulatory relationships between genes involved in the choice between neural and mesoderm fates.

Keywords

Mouse embryo; primitive streak; gastrulation; paraxial mesoderm; neural ectoderm; somite; EMT; progenitor cells; Wnt3a; Msgn1; Tbx6

Introduction

The paraxial mesoderm is one of the subpopulations of mesoderm emerging from the primitive streak (PS) at gastrulation. The skeletal muscles and vertebral column, comprising the axial musculature and axial skeleton, are derived from paraxial mesoderm. At the PS, pluripotent epiblast cells, ingress and undergo an epithelial-to-mesenchymal transition (EMT), and subsequently migrate away as nascent mesoderm (Nowotschin and Hadjantonakis, 2010). As ingression proceeds, columnar epithelial epiblast cells break down their basement membrane, disassemble cell-cell junctions (tight and adherens junctions),

*Corresponding author at: Sloan Kettering Institute, Developmental Biology Program, 1275 York Ave, new York, NY 10065, USA. Phone: 212-639-3159. Fax: 646-422-2355, hadj@mskcc.org (Kat Hadjantonakis).

detach from the epithelium and extend filopodia (Ferrer-Vaquer et al., 2010). The time and location where cells ingress into and emerge from the primitive streak, dictates the subtype of mesoderm they will form: extra-embryonic, cardiac, axial or paraxial as well as lateral plate and intermediate mesoderm (Kinder et al., 1999).

The paraxial mesoderm is believed to be the final population to exit the streak. Moreover, production of paraxial mesoderm continues after germ layer formation, and what is generally thought of as gastrulation, ceases. At these later stages, paraxial mesoderm is formed within the tail bud, the structure evolving from and replacing the PS. In this way, the tail bud serves as a source of mesodermal cells up until at least E11.5, long after the PS has regressed (Cambray and Wilson, 2002; Gont et al., 1993). During axis elongation paraxial mesoderm becomes segmented into paired epithelialized blocks of cells, the somites. The somites eventually differentiate into dermamyotome and sclerotome, which give rise to the dermis (skin), axial skeletal muscles and the axial skeleton, respectively. Precise somite segmentation is ensured by an intrinsic molecular oscillator, involving a dynamic clock and wavefront mechanism dependent on the integration of Wnt and Fgf signaling (Dubrulle and Pourquie, 2004; Naiche et al., 2011; Pourquie, 2001).

Formation of most rostral (also referred to as anterior) somites, comprising somites 1 to ~7, appears to be distinct from majority of the somites (somites >7), also referred to as the posterior somites (Pourquie, 2001). A large number of mutants affecting the morphogenesis of paraxial mesoderm have been described (Pourquie, 2001). These mutants disrupt genes encoding a variety of factors ranging from signaling pathway components, cell adhesion molecules and extracellular matrix components, to transcription factors and cell cycle regulators. However, some general principles have emerged. The Wnt, Fgf and Delta/Notch signaling pathways have been shown to play important, and often reiterative, roles in paraxial mesoderm formation and somite segmentation (Pourquie, 2001).

In this study we have focused on three critical factors for paraxial mesoderm formation; Wnt3a, a member of the Wnt family of signaling proteins, the basic-Helix-Loop-Helix (bHLH) transcription factor Mesogenin1 (Msgn1), and the T-box transcription factor Tbx6 (Chalamalasetty et al., 2011; Chapman et al., 1996; Chapman and Papaioannou, 1998; Takada et al., 1994; Wittler et al., 2007; Yoon et al., 2000; Yoon and Wold, 2000). All three genes are specifically expressed within the primitive streak and mutations result in profound loss of paraxial mesoderm and posterior somites.

Mutants in *Wnt3a, Msgn1* and *Tbx6* have been reported to exhibit a complete absence of paraxial mesoderm posterior to somite 6/7, and aberrant morphogenesis of the anterior (1-6/7) somites (Chapman and Papaioannou, 1998; Takada et al., 1994; Yoon and Wold, 2000). Another unique phenotype observed in both *Wnt3a* and *Tbx6,* but not *Msgn1,* mutants is the formation of ectopic neural tubes concomitant with the absence of paraxial mesoderm/posterior somites (Chapman and Papaioannou, 1998; Yoshikawa et al., 1997). A feature observed in all three mutants is a morphologically distinct tail bud. *Wnt3a* mutants are characterized by a tail bud of reduced size, suggesting a depletion of cells. By contrast, *Msgn1* and *Tbx6* mutants possess an enlarged tail bud, presumably resulting from the accumulation of mesoderm cells that likely fail to migrate away from their place of origin, suggesting a failure in cell specification (Chapman and Papaioannou, 1998; Yoon and Wold, 2000). The phenotypic similarities among these three mutants have led to the hypothesis that all three factors converge in the same regulatory network necessary for the specification, proliferation, emergence and segmentation of the paraxial mesoderm. Notably, even though these single mutant phenotypes have previously been individually described, no detailed direct comparison has been reported. Moreover, the epistatic relationship between these

three genes, their possible genetic interactions, as well as their specific roles within the paraxial mesoderm lineage remain to be fully understood.

Previous studies have suggested that *Wnt3a* acts upstream in this hierarchy of paraxial mesoderm specification. Together with Fgf receptor 1 (Fgfr1), Wnt3a controls the expression of another T-box gene *T*, which has a role in the formation of all posterior mesoderm, but in the context of paraxial mesoderm regulates *Tbx6* expression (Hofmann et al., 2004). On the other hand, Wnt signaling together with Tbx6 is important for controlling the expression of the Notch1 ligand, *Dll1*, during somite segmentation (Chapman and Papaioannou, 1998; Hrabe de Angelis et al., 1997). *Msgn1* has been shown to be a target of Tbx6 and Wnt signaling, placing it downstream in the signaling cascade, *Tbx6* expression in the paraxial mesoderm, in turn, has been shown to be Wnt signaling dependent (Chalamalasetty et al., 2011; Takemoto et al., 2011; Wittler et al., 2007). While much effort has been invested in unraveling this gene regulatory network controlling paraxial mesoderm morphogenesis, previous studies have primarily relied on analyses of *cis*-regulatory elements using transgenic methods. To validate the roles of *Wnt3a*, *Tbx6* and *Msgn1* in the genetic hierarchy regulating paraxial mesoderm formation, we have performed a genetic study by analyzing single and compound mutants of these three factors. Our data suggest a complex interplay between these three key factors that cannot be simply explained by current models, which are based solely on the analysis of single mutants and promoter binding activities.

To begin to unravel the details of this complex network, we first determined the detailed comparative spatial and temporal patterns of expression of *Wnt3a*, *Msgn1* and *Tbx6* at a time when paraxial mesoderm is being formed. We determined whether these three factors are co-expressed or complementarily expressed within cells of the primitive streak and emergent paraxial mesoderm. Then, we investigated their epistatic relationship by analyzing double mutant embryos and compared their phenotypes to the single mutants to gain insight into the sequential hierarchical requirements for these factors within the paraxial mesoderm lineage. Finally, through the analysis of molecular markers in mutants, our data reveal that: (1) progenitor cells of the paraxial mesoderm cells are bipotential. As suggested by recent lineage tracing experiments (Tzouanacou et al., 2009), these progenitors can adopt a neural or mesodermal fate, a decision regulated by the intricate interplay of all three factors, and that (2) distinct molecular pathways are in place during anterior and posterior somite formation.

Materials and methods

Mouse strains and embryo collection

Mutant strains used in this study were *Wnt3a* (JAX Strain Name: B6.129S1-Wnt3a^{tm1Amc}/J, JAX IMR Stock number:004581) (Takada et al., 1994) *Msgn1* (a gift of J.K. Yoon, Maine Medical Center Research Institute, USA) (Yoon and Wold, 2000) and *Tbx6*$^{H2B\text{-}EYFP}$, a knock-in reporter strain harboring an H2B-EYFP fusion cassette (Hadjantonakis et al., 2008; Nowotschin et al., 2009) targeted to the *Tbx6* locus which recapitulates *Tbx6* promoter activity while ablating gene function. For this *Tbx6* allele an *H2B-EYFPpA-lox*P-*PGK-NeopA-lox*P cassette was targeted into exon 1, replacing the endogenous ATG with that of the H2B-EYFP fusion reporter, while deleting exon 2 and part of exon 3. The H2B-EYFP fusion destroys gene function and produces animals exhibiting an identical mutant phenotype to previously described alleles (Chapman and Papaioannou, 1998; Garcia-Garcia et al., 2005) while reporting *Tbx6* promoter activity (Hadjantonakis et al., 2008) and our unpublished observations). *Wnt3a*, *Msgn1* and *Tbx6* mutants were intercrossed to collect double and single mutant embryos. To circumvent any defects that might be present in heterozygous animals wild-type controls were used in all experiments. Embryos were

collected from timed matings with the day of the vaginal plug being considered as E0.5 and, additionally, staged by somite number or by morphology of head and heart. A minimum of three embryos of each genotype was examined for each time point or probe. The genotype of embryos was confirmed by PCR using the following primers: *Wnt3a:* 5′-TTTTGGACTACAACCCTCCTCACCTGG-3′, 5′-AGCCTCATTGTTGTGACGGTTC-3′ and 5′-TGGCTACCCGTGATATTGCT-3′; *Msgn1*: 5′-CCAAGGAGCCTTGTACTGCTGC-3′, 5′-GCCACCAGCAGTGTGTAGATAGGGAGGT-3′ and 5′-GCAAAGCGCCATTCGCCATTC-3′; *Tbx6*: 5′-ATTGCACGCAGGTTCTCCGG-3′; 5′-GTCACGACGAGATCCTCGCC-3′; 5′-GTACCATCCACGAGAGTTGTAC-3′.

In situ hybridization (ISH)

Embryos were dissected in DMEM/F12 (1:1) and fixed in 4% paraformaldehyde overnight at 4°C, washed in PBS$^{-Ca2+,-Mg2+}$/0.1% Tween-20 and dehydrated through a methanol series into 75% Methanol. Whole mount ISH was performed as previously described using antisense riboprobes to *Msgn1* (Yoon et al., 2000), *Tbx6* (Chapman et al., 1996), *Wnt3a* (Parr et al., 1993) and *Mox1* (Candia et al., 1992).

Immunofluorescence (IF)

Embryos were dissected in DMEM/F12 (1:1) and fixed in 4% paraformaldehyde overnight at 4°C for F-Actin and Hoechst staining or for 20 min at room temperature for antibody staining followed by two washes in PBS. Antibodies used: Sox2 (1:50 dilution, R&D) and cleaved Caspase-3 (1:200 dilution, Cell Signaling Tech). For cryosectioning embryos were equilibrated in 15% Sucrose/PBS for 1 hour, 30% Sucrose/PBS overnight at 4°C, and embedded in Tissue-Tek OCT (Sakura Finetek). Cryosections (12 μm) were cut on a Leica CM3050 cryostat. Sections were washed in PBS, counterstained with Hoechst to label nuclei (1:1000, Invitrogen) and Alexa-633 Phalloidin for labeling F-actin (1:500, Invitrogen). Cryosections were blocked for 1 hour in 0.5% Triton X-100/10% FBS/PBS. Secondary antibodies used were Alexa-Fluor 568 and 488 (1:500 dilution, Invitrogen). Whole mount IF was performed as previously described (Kwon et al., 2008).

Histology

Mouse embryos were dissected in DMEM/F12, fixed overnight in 4% paraformaldehyde, washed 3X in PBS$^{-Ca2+,-Mg2+}$, dehydrated in a graded ethanol/xylene series and embedded in paraffin. Sections (7μm) were stained with hematoxylin and eosin according to standard protocols.

Imaging

Widefield images of whole mounts were acquired with an Axiocam MRc CCD camera (Zeiss) mounted on a Leica MZ165FC stereo microscope. Images of H&E sections and sections of ISH were acquired with an Axiocam MRc CCD camera (Zeiss) mounted on a Zeiss Axioscope A1 in bright field or DIC mode, respectively. Laser scanning confocal images of immunostained sections and whole mounts were acquired on a LSM510 META (Zeiss). Fluorescence was excited with a 405 nm diode laser (Hoechst), a 488 nm Argon laser (EYFP), a 543 nm HeNe laser (Alexa Fluor 568) and a 633 nm HeNe laser (Alexa Fluor 633). Images were acquired using a Plan-Apo 20x/NA0.75 and Fluar 5x/NA0.25 objectives. Raw data were processed using AIM software (Zeiss) and assembled in Photoshop CS4 (Adobe).

Results

Profound loss of posterior paraxial mesoderm and absence of posterior somites in Wnt3a$^{-/-}$, Tbx6$^{-/-}$ and Msgn1$^{-/-}$ mutants

The paraxial mesoderm marker *Mox1* revealed loss of posterior somites, the hallmark of *Wnt3a*$^{-/-}$, *Tbx6*$^{-/-}$ and *Msgn1*$^{-/-}$ mutants at the 16–18ss (Figure 1B–D, 1B′–D′) compared to the wild-type (Figure 1A and 1A′). At earlier stages (10ss) smaller and aberrant anterior somites were observed in *Wnt3a*$^{-/-}$ and *Tbx6*$^{-/-}$ mutants (Figure 1F, 1F′, 1H and 1H′). *Msgn1*$^{-/-}$ mutants exhibited no readily detectable defect in anterior somites and loss of posterior somites is only found after segmentation of somite 11 (Figure 1G and 1G′) in contrast to complete loss of posterior somites observed in *Wnt3a*$^{-/-}$ and *Tbx6*$^{-/-}$ mutants. These defects were in agreement with previous characterizations of each of these three mutants (Chapman and Papaioannou, 1998; Takada et al., 1994; Yoon and Wold, 2000).

Dynamic but distinct patterns of expression of Tbx6, Msgn1 and Wnt3a within the primitive streak and presomitic mesoderm

We reasoned that a prerequisite to undertaking a comparative analysis of *Wnt3a*, *Msgn1* and *Tbx6* mutants was a detailed analysis of the expression of these three genes in wild-type embryos. At early bud (EB) stage as well as in late bud (LB) stages *Tbx6* and *Wnt3a* were restricted to the posterior side of the embryo in the vicinity of the primitive steak (PS) (Figure 2A, 2B, 2G, 2H). By contrast, primitive streak-specific *Msgn1* expression lagged that of *Wnt3a* and *Tbx6* and was only detected by the LB stage (Figure 2E). Of note, onset of *Msgn1* expression did occur at the EB stage, but was restricted to the allantoic bud (Figure 2D).

At the headfold stage (HF) all three genes continued to be expressed in the primitive streak region (Figure 2C1–4, 2F1–4, 2I1–4). *Wnt3a* was expressed in epiblast cells surrounding the site of cell ingression (Figure 2C3–4) and was maintained in recently ingressed cells located posteriorly/dorsally in the presomitic mesoderm (PSM) (Figure 2C3–4). This distinct pattern of expression of *Wnt3a* was maintained throughout axis elongation from the HF stage up until late somite stages (>19ss) (Figure 2C, 2J, 2K and 2L). At the HF stage *Tbx6* was predominantly expressed in a medial-lateral domain within the nascent mesoderm, the wings of nascent mesoderm, as well as in a few epiblast cells at the site of cell ingression where it overlapped with *Wnt3a* (Figure 2I1–4). *Tbx6* ceased to be expressed in epiblast cells coincident with the start of somite segmentation. At that time its expression was restricted to PSM cells. In the rostral part of the PSM *Tbx6* was expressed dorsally adjacent to the neural plate, whereas it could be found in the entire mesoderm cell population in more caudal regions, close to the caudal lateral epiblast (CLE) of the tail region (Figure 2P, 2Q and 2R).

Msgn1 was unique in that at the HF stage it was exclusively expressed in the mesoderm, where it overlapped in part with *Tbx6* (Figure 2F1–4). However, *Tbx6* expression extended farther laterally from the streak into the PSM (Figure 2I3–4). At early through late somite stages *Msgn1* continued to be expressed in PSM cells throughout the tail region but was predominantly caudally restricted, and similar to *Tbx6* expression (Figure 2N3, 2O3).

Of all the three genes, expression of *Tbx6* extended most anteriorly, being localized throughout the PSM and ending abruptly at its rostral border where somites segment (Red arrowheads, Figure 2Q1–2, 2R1–2). By contrast, the expression domain of *Msgn1* did not encompass the full rostro-caudal length of the PSM and predominated posteriorly (Figure 2N1–2, 2O1–2). The domain of *Wnt3a* expression was limited to the caudal end of the PSM (Figure 2K1–2, 2L1–2).

The partially overlapping, as well as distinct, domains of expression of *Wnt3a*, *Tbx6* and *Msgn1* suggest multiple intersecting, as well as unique, roles for these three factors in presomitic mesoderm lineage specification and morphogenesis.

Defects of intermediate or greater severity in double mutant embryos evident by gross morphology

We next sought to establish whether these factors were acting hierarchically within the paraxial mesoderm lineage. To do so, we tested the genetic interactions between the three factors by analyzing the phenotype of embryos from double mutant crosses and comparing them with single mutants. Even though the phenotypes of embryos lacking *Wnt3a*, *Msgn1* or *Tbx6* have previously been individually described, demonstrating that all three genes are necessary for paraxial mesoderm specification and/or morphogenesis (Chapman et al., 2003; Chapman and Papaioannou, 1998; Takada et al., 1994; Yoon and Wold, 2000), the epistatic relationship between these three genes, their possible genetic interactions, as well as their specific roles in paraxial mesoderm specification have not been clearly deciphered.

We assessed the gross morphology of the single mutants and all combinations of double mutant embryos in whole mount at the 10–12ss (Figure 3), in H&E stained histological sections at the 10–12ss (Figure 4), as well as in F-Actin and nuclear stained sections of 10–12ss and 20–25ss embryos (Supplemental Figure 1). *Wnt3a*$^{-/-}$ mutants exhibited the reported phenotype (Takada et al., 1994). Posterior somites were absent and the size of the tail region was reduced (Figure 3B–B2, Figure 4B–B3) at 10–12ss, as well as at 20–25ss. Of the anterior somites (somites 1–7), the most rostral developed normally whereas the more caudal ones were diminished in size or absent (Figure 3B1). We also noted that the neural tube of *Wnt3a*$^{-/-}$ mutants was kinked, albeit to a lesser extent than previously reported (Takada et al., 1994). The notochord was absent in the posterior region of the embryo (Supplemental Figure 1I2). At later stages, 20–25ss, an ectopic neural tube positioned ventrally to the axial neural tube was observed (Supplemental Figure 1I2). In addition to these previously described defects, we also noted presumptive neural cells apparent by their epithelial morphology and Sox2 expression positioned laterally to the axial neural tube, located in close proximity to the ventral neural tube (green arrowheads in Supplemental Figure 1I2, also see Figure 6B3–4, Figure 7B3–4).

The *Msgn1*$^{-/-}$ mutant was characterized by an enlarged tail region (Figures 3C, 3C2, 4C, 4C3) (Yoon et al., 2000; Yoon and Wold, 2000) and kinked neural tube (Figure 3C1). The anterior somites (somites 1–7) formed normally, the subsequent somites (somites 8–11), were aberrant in morphology and small in size, while no somites formed posterior to these. There was a marked reduction of paraxial mesoderm tissue in this region (Figure 3C1 and Supplemental Figure 1C2, J2) and vascular blebs (Figure 3C1) were present on the dorsal side of the trunk. These blebs likely give rise to the ectopic pools of blood observed at later stages (20–25ss) as previously noted (Yoon and Wold, 2000). The notochord was not affected in the *Msgn1*$^{-/-}$ mutant (Figure 4C1–C2).

Of the three mutants affecting the paraxial mesoderm, the *Tbx6*$^{-/-}$ mutant, displayed the most severe somite segmentation defect. The most anterior somites were reduced in size, and aberrantly formed. There was a complete absence of all posterior somites (Figure 3D1); the tail region was enlarged (Figure 3D, 3D2, 4D3) and comprised undifferentiated mesenchymal cells. As previously reported, in the posterior region of the trunk ectopic neural tubes flanked the axial (primary) neural tube (Figure 4D2) suggesting that cells exiting the primitive streak had either adopted a neural fate or remained within the tail bud in an undifferentiated state, resulting in formation of an enlarged tail bud (Chapman and Papaioannou, 1998). No defects were observed in the formation in the notochord in the *Tbx6*$^{-/-}$ mutant.

Previous studies have suggested that Wnt3a acts upstream in a genetic network within the paraxial mesoderm lineage regulating *Tbx6* and *Msgn1* expression (Wittler et al., 2007). However, the phenotype of *Tbx6*$^{-/-}$ and *Msgn1*$^{-/-}$ single mutants is not identical to the *Wnt3a*$^{-/-}$ mutant suggesting the hierarchy of interactions between these three factors is more complex than simple epistasis.

As in the *Wnt3a*$^{-/-}$ single mutant, the anterior somites of *Wnt3a*$^{-/-}$*; Msgn1*$^{-/-}$ mutants formed, but they were aberrant, whereas posterior somites were completely missing (Figure 4E–E3). The tail region of *Wnt3a*$^{-/-}$*; Msgn1*$^{-/-}$ embryos was reduced in size (Figure 3E, 3E2). However, it contained more mesoderm cells than in the *Wnt3a* mutant, suggesting that some cells were able to ingress through the primitive streak (Figure 4E3; see also Figure 6E1). Using *T* as a pan-mesodermal marker (Supplemental Figure 2) we observed more mesoderm in the primitive streak region in *Wnt3a*$^{-/-}$*; Msgn1*$^{-/-}$ compared with *Wnt3a*$^{-/-}$ and *Wnt3a*$^{-/-}$*; Tbx6*$^{-/-}$ embryos. Like in the *Wnt3a* mutant (Takada et al., 1994), the notochord was absent in the posterior of the trunk. The neural tube was more kinked (Figure 3E1) as compared to the *Wnt3a*$^{-/-}$ single mutant, though less severe than in the *Msgn1*$^{-/-}$ mutant (Figure 3C1). Vascular blebs, a hallmark of the *Msgn1*$^{-/-}$ single mutant (Figure 3C1), were not detected in *Wnt3a*$^{-/-}$*; Msgn1*$^{-/-}$ double mutant embryos. Of note, amorphous clusters of densely packed cells were observed dorsal to, and ventral to, the axial neural tube. These cells were not detected in either of the single mutants (Figure 4E1–E2; Table 1).

Wnt3a$^{-/-}$*; Tbx6*$^{-/-}$ double mutants displayed a generally more severe phenotype than either of the single mutants. As in *Wnt3a*$^{-/-}$ single mutants, the double *Wnt3a*$^{-/-}$*; Tbx6*$^{-/-}$ mutants exhibited a reduced tail region (Figure 3F, 3F2). The neural tube in the *Wnt3a*$^{-/-}$*; Tbx6*$^{-/-}$ was severely kinked and no notochord was detected in the posterior part of the embryo. With the exception of the most anterior somites, which were small and lacked the stereotypical organization, somites were absent (Figure 3F1, 4F1–F2; Table 1).

By contrast to the other two double mutant combinations, both of which contained a *Wnt3a*$^{-/-}$ allele, *Msgn1*$^{-/-}$*; Tbx6*$^{-/-}$ embryos displayed an enlarged tail region characteristic of both *Msgn1*$^{-/-}$ and *Tbx6*$^{-/-}$ single mutants (Figure 3G, 3G2, 4G3). The neural tube was very kinky. Moreover, the loss of paraxial mesoderm tissue along the rostro-caudal axis of the posterior trunk was more severe than in either of the single mutants (Figure 3G1, Figure 4G1–G2). Lateral ectopic neural tubes, as found in the *Tbx6*$^{-/-}$ mutant, were present (see Figure 8A1–3, Table 1). They were, however, smaller in size. As in the *Wnt3a*$^{-/-}$*; Msgn1*$^{-/-}$ mutants, amorphous cell accumulations were observed adjacent to the axial neural tube throughout the posterior trunk region, as well within the neural tube (Figure 4G1–G2), suggesting a misspecification of mesoderm cells into neural tissue. Since these ectopic clusters of cells were only observed in double mutants containing a null allele of *Msgn1,* it would suggest a role for *Msgn1* in cell migration away from the primitive streak.

Two distinct gene regulatory networks regulating anterior and posterior somite formation involving reciprocal interactions between Wnt3a, Tbx6 and Msgn1

To understand the genetic regulation between *Wnt3a*, *Tbx6* and *Msgn1*, we analyzed the expression of each factor in single as well as in double mutants at the 8–10ss. Upregulation of *Wnt3a* expression was detected in *Msgn1*$^{-/-}$ (Figure 5F1–F2) and in *Tbx6*$^{-/-}$ mutants (Figure 5H1–H4) suggesting a negative feedback loop of both transcription factors on *Wnt3a. Wnt3a* expression in the *Tbx6*$^{-/-}$ mutant was upregulated in cells of the neural plate, primitive streak and tail region that express *Wnt3a* in a wild-type context (Figure 5A3–4 and 5H3–4), whereas ectopic expression of *Wnt3a* was observed in the tail region and the neural tube of *Msgn1*$^{-/-}$*; Tbx6*$^{-/-}$ double mutants (Figure 5J1–J2). Sections revealed *Wnt3a* expression along the entire neural tube, as well as in the cells of the tail region in a

peripheral pattern. Of note, the ectopic cell clusters observed in close proximity to the neural tube were also positive for *Wnt3a* (Figure 5J6). Analysis of *Msgn1* revealed its downregulation in the PSM of *Tbx6*$^{-/-}$ mutants (Figure 5I1–I2) and a complete absence in the PSM of the *Wnt3a*$^{-/-}$ (Figure 5D1–D2), as well as in the *Wnt3a*$^{-/-}$*; Tbx6*$^{-/-}$ mutants (Figure 5K1–K2), suggesting that *Msgn1* acts downstream of both Wnt3a and Tbx6 in the majority of the paraxial mesoderm cells. On the other hand, *Tbx6* expression was completely lost in both, *Wnt3a*$^{-/-}$ and *Msgn1*$^{-/-}$ single mutants (Figure 5E1–E2; 5G1–G2) and consequently in the *Wnt3a*$^{-/-}$*; Msgn1*$^{-/-}$ at the stage analyzed (Figure 5L1–L2).

Given the different phenotypes of the *Wnt3a*$^{-/-}$*; Msgn1*$^{-/-}$ and *Wnt3a*$^{-/-}$*; Tbx6*$^{-/-}$ mutants, we hypothesized that one of them might phenocopy a triple mutant. To address this hypothesis, we performed ISH at early stages, from headfold to 0ss (Supplemental Figure 3), and found that neither *Msgn1* was downregulated in *Wnt3a*$^{-/-}$*; Tbx6*$^{-/-}$ mutants (Supplemental Figure 3D, I and K) nor *Tbx6* in *Wnt3a*$^{-/-}$, *Msgn1*$^{-/-}$ (Supplemental Figure 3 E, G and L) at these early stages. These data, therefore, suggest that neither *Wnt3a*$^{-/-}$*; Msgn1*$^{-/-}$ nor *Wnt3a*$^{-/-}$*; Tbx6*$^{-/-}$ mutants are in effect triple mutants, and that early (anterior) somite formation requires a molecular pathway that is distinct from posterior somite formation.

Expansion of Sox2 expression in double and single mutants

Both *Tbx6*$^{-/-}$ and *Wnt3a*$^{-/-}$ single mutants, as well as the three double mutant combinations were characterized by the presence of ectopic lateral and/or ventral neural tubes (Figure 6 and 7). We analyzed the expression of the neural and pluripotency marker Sox2 in these ectopic structures at early somite stages (10–12ss, Figure 6), as well as at later somite stages (20–25ss, Figure 7).

In early to late somite stage wild-type embryos Sox2 was localized to cells within the primitive streak (Figure 6A1–A2, 7A1–A2), as well as cells of the axial (primary) neural tube (Figure 6A3–A4, 7A3–A4). In *Wnt3a*$^{-/-}$ and *Msgn1*$^{-/-}$ single mutants cells of the primitive streak region were Sox2-positive (Figure 6B1–B2, 6C1–C2), whereas by the 20–25ss stage, Sox2 was not detected in the tail bud region of either, *Wnt3a*$^{-/-}$ or *Msgn1*$^{-/-}$ single mutants (Figure 7B1–B2, 7C1–C2). Cells of the axial neural tube were Sox2-positive in both mutants at both early and late somite stages (Figure 6B3–B4, 6C3–C4, 7B3–B4, 7C3–C4). However, additional sites of expression of Sox2 were not only present in the ventral neural tube at the 20–25ss (Figure 7B3–B4) but also in the cell clusters occurring lateral to the axial neural tube in *Wnt3a*$^{-/-}$ mutants at both early and late somite stages (Figure 6B3–B4, 7B3–B4). Notably, these Sox2-positive rosette-like clusters of cells always maintained an attachment to the axial neural tube and did not form proper tube-like structures compared to the ectopic lateral tubes observed in the *Tbx6*$^{-/-}$ mutant. As recently reported by the study of Takemoto et al. (Takemoto et al., 2011), we also detected ectopic expression of Sox2 in the tail region of *Tbx6*$^{-/-}$ single mutants at early and late somite stages (Figure 6D1–D2, 7D1–D2). In addition, cells of the ectopic lateral neural tubes were Sox2-positive (Figure 6D3–D4, 7D3–D4).

Sox2 was observed in the cells of the primitive streak at 10–12ss in *Wnt3a*$^{-/-}$*; Msgn1*$^{-/-}$ and *Wnt3a*$^{-/-}$*; Tbx6*$^{-/-}$ double mutants (Figure 6E1–E2, 6F1–F2). However, no Sox2 expression was detected in the tail bud of these mutants at later stages (Figure 7E1–E2, 7F1–F2). Sox2 was detected in the axial neural tube as well as in the ventral neural tube at early and late somites stages in *Wnt3a*$^{-/-}$*; Msgn1*$^{-/-}$ and *Wnt3a*$^{-/-}$*; Tbx6*$^{-/-}$. However, the levels of expression of Sox2 within these structures were not as high as compared to the single mutant counterparts (Figure 6E3–E4, 6F3–F4; Figure 7E3–E4, 7F3–F4).

Analysis of Sox2 in *Msgn1*$^{-/-}$; *Tbx6*$^{-/-}$ mutants revealed its ectopic expression within the primitive streak region at early somite stages (Figure 6G1–G2), and at 20–25ss in the tail bud region encompassing almost the entire cell population of the tail bud (Figure 7G1–G2). More anteriorly, Sox2 was detected in the axial neural tube at early and late somite stages (Figure 6G3–G4, 7G3–G4). Moreover, analysis of Sox2 expression along the rostro-caudal axis of *Msgn1*$^{-/-}$; *Tbx6*$^{-/-}$ mutants at the 20–25ss (Figure 8) revealed expression in lateral ectopic neural tubes anteriorly which were smaller than those observed in *Tbx6*$^{-/-}$ mutants (Figure 7D3–D4). Cells of the kinked axial neural tube were Sox2-positive (Figure 8B2–B3 and 8C2–C3), as were the ectopic cell clusters, which were located dorsal or internal to the axial neural tube (Figure 8C2–C3 and 8D2–D3). Notably, some of these clusters could be distinguished from cells within the neural tube by their elevated but non-polarized distribution of F-Actin (Figure 8C1)

A more detailed investigation of the cells within the tail bud of the *Tbx6*$^{-/-}$ and *Msgn1*$^{-/-}$; *Tbx6*$^{-/-}$ mutant revealed cells in a particular region in the tail bud of *Msgn1*$^{-/-}$; *Tbx6*$^{-/-}$, but not *Tbx6*$^{-/-}$ at 20–25ss lacking Sox2 expression and underwent apoptosis as evident by both Hoechst nuclear and activated-Caspase staining (Figure 8E–G). By contrast, a population of cells undergoing apoptosis was not observed in *Msgn1*$^{-/-}$ nor *Tbx6*$^{-/-}$ single mutants at that stage (data not shown).

Discussion

The axial musculature and skeleton are derived from paraxial mesoderm, a tissue emanating from the primitive streak and tail bud in the mouse embryo. In this study we have focused on three critical components of the gene regulatory network operating during paraxial mesoderm formation in the mouse. Since *Wnt3a*, *Msgn1* and *Tbx6* are single gene mutations that exhibit a profound loss of paraxial mesoderm tissue, and display complete absence of posterior somites, we reasoned that a genetic analysis of these three mutants would provide insight into the hierarchical and reciprocal activities of these three factors.

Wnt3a promotes cell ingression and functions as a guidepost for paraxial mesoderm cells

Our analysis of *Wnt3a*, *Tbx6* and *Msgn1* expression patterns in wild-type and mutant embryos, as well as the analysis of double mutant embryos support a model in which *Wnt3a* is positioned at the top of the genetic network controlling paraxial mesoderm formation. Of these three key factors, *Wnt3a* and *Tbx6* are the first genes to be expressed within the primitive streak region, being activated at the early bud stage. *Wnt3a* exhibits a graded expression across the primitive streak; being predominantly expressed in dorsal cells, and to a lesser extent in the emergent mesoderm. These data reveal that cells modulate the expression of *Wnt3a* as they traverse the primitive streak. As they enter, they upregulate, and subsequently downregulate *Wnt3a* as they exit. *Wnt3a*$^{-/-}$ mutants exhibit a reduced tail bud stemming from defects in the first steps of late paraxial mesoderm formation such as ingression/EMT suggesting an early role of Wnt3a in that process (Figure 9).

Tbx6 exhibits a reciprocal pattern of expression to *Wnt3a*, whereby its expression peaks within the mesoderm, but it is also detected in few cells of the epiblast, suggesting that these cells may be ingressing or transitioning through the primitive streak. Alternatively, they may have committed to ingress, and in doing so activated this T-box transcription factor. *Tbx6* is therefore expressed in cells that are expressing *Wnt3a*. *Tbx6* and *Msgn1* are downregulated in the *Wnt3a* mutant, as well as in the respective double mutants. This places them downstream of *Wnt3a*. In *Tbx6*$^{-/-}$ and *Msgn1*$^{-/-}$ mutants, processes, such as PSM specification and cell migration that lie downstream of ingression/EMT are affected. Both mutants exhibit an enlarged tail bud suggesting that ingression/EMT is taking place. However, in both mutants cells cannot properly become specified into paraxial mesoderm

and/or they cannot migrate out of the tail bud to subsequently undergo segmentation into somites (Figure 9).

The phenotypes of both, *Wnt3a*$^{-/-}$; *Tbx6*$^{-/-}$ and *Wnt3a*$^{-/-}$; *Msgn1*$^{-/-}$, double mutants exhibited a predominantly *Wnt3a* mutant phenotype, which is characterized by a severe reduction in size of the tail region. However, closer examination revealed that the *Wnt3a*$^{-/-}$; *Tbx6*$^{-/-}$ double mutants exhibited a more severe phenotype than the single *Wnt3a* mutant. The formation of anterior somites was more severely affected as well as the kinkiness of the neural tube compared to the single mutants (Table 1). Though both Tbx6 and Msgn1 are absent at later somite stages in *Wnt3a*$^{-/-}$; *Msgn1*$^{-/-}$ and *Wnt3a*$^{-/-}$; *Tbx6*$^{-/-}$ double mutants curiously neither of them is an effective triple mutant since at head fold and early somite stages *Tbx6* and *Msgn1* are still expressed and must be regulated by other factors than Wnt3a. The intermediate phenotype of *Wnt3a*$^{-/-}$; *Msgn1*$^{-/-}$ characterized by both an intermediate level of kinkiness of the neural tube and size of tail region that is reduced but not as severely as in the *Wnt3a*$^{-/-}$ mutant and the different phenotypes of *Wnt3a*$^{-/-}$; *Msgn1*$^{-/-}$ and *Wnt3a*$^{-/-}$; *Tbx6*$^{-/-}$ (Table 1) could be explained by early and distinct roles of Msgn1 and Tbx6. Furthermore, presence of expression of *Msgn1* and *Tbx6* in the *Wnt3a*$^{-/-}$ mutants shows that the activation of both genes in the early phase of somite formation is mostly Wnt3a independent (Figure 10). In sum, the expression of *Wnt3a* within cells of the primitive streak, as well as the absence of *Tbx6* and *Msgn1* at later stages, and reduced size of the tail region in *Wnt3a*$^{-/-}$ mutants, reveals an indispensable role for Wnt3a during ingression of cells through the primitive streak or in the maintenance of a stem or progenitor cell population resident within the primitive streak, and in posterior somite formation (Figure 9, 10). However, during the formation of the anterior somites it plays a less prominent role. The positive regulatory loop of *T* and *Wnt3a* (Yamaguchi et al., 1999) and the regulation of *Tbx6* by *T* (Chapman et al., 1996; Chapman et al., 2003) is compatible with this interpretation.

Tbx6 represses neural fate and promotes paraxial mesoderm specification in cells of the tail bud

Our results reveal that the neural and pluripotency marker Sox2 is upregulated in *Tbx6* expressing cells within the tail bud of *Tbx6*$^{-/-}$ mutants, as well as in *Msgn1*$^{-/-}$; *Tbx6*$^{-/-}$ double mutants. These results reveal that Tbx6 must be functioning in a genetic circuit with Sox2, as only cells that would normally express Tbx6 upregulated Sox2. Furthermore, the ectopic upregulation of Sox2 could account for the ectopic lateral neural tubes observed in *Tbx6* mutants, as well the lateral ectopic neural tubes and marked expansion of neural tissue within the axial neural tube, leading to a very severely kinked tube in *Msgn1*$^{-/-}$; *Tbx6*$^{-/-}$ double mutants.

In agreement with our observations, a recent report has shown that Tbx6 regulates *Sox2* through indirect repression of its N1 enhancer (Takemoto et al., 2011; Uchikawa et al., 2003) (Figure 9). The N1 enhancer is regulated by Wnt and Fgf signaling, and is active in the caudal lateral epiblast (CLE), a region of the embryo proposed to harbor a bipotential axial stem cell population giving rise to both, neural and mesodermal cells (Tzouanacou et al., 2009; Wilson et al., 2009). Deletion of the N1 enhancer sequence in *Tbx6* mutants (*Tbx6*$^{-/-}$; *Sox2*$^{\Delta N1/\Delta N1}$) uncoupled the two aspects of the phenotype, as it resulted in absence of paraxial mesoderm, but without formation of ectopic neural tubes. Thus repression of *Sox2* in a *Tbx6*$^{-/-}$ mutant rescued the ectopic neural tube defect, but not the absence of paraxial mesoderm (Takemoto et al., 2011). Since these two defects can be uncoupled, it suggests the absence of paraxial mesoderm is independent of Sox2 repression. This raises the question of the identity of the cells that can neither adopt a neural nor paraxial mesoderm identity in *Tbx6*$^{-/-}$; *Sox2*$^{\Delta N1/\Delta N1}$ embryos. Might these cells be trapped in a transition state, as a result of an inability to differentiate? Given our observations, it is

also tempting to speculate whether the *Tbx6*$^{-/-}$*; Sox2*$^{\Delta N1/\Delta N1}$ mutant might phenocopy the *Msgn1*$^{-/-}$ mutant.

However, Sox2 overexpression in the CLE cannot account for the ectopic neural tissue observed in other mutants, including the ventral neural tube and amorphous clusters of cells observed in the *Wnt3a*$^{-/-}$ as well as in *Wnt3a*$^{-/-}$*; Msgn1*$^{-/-}$ and *Wnt3a*$^{-/-}$*; Tbx6*$^{-/-}$ double mutants. This could suggest either that other Wnt signaling factors expressed in this region of the embryo compensate for Wnt3a in the activation of Sox2, or that the default fate of cells that cannot ingress through the streak is to adopt neural identity.

Msgn1 is essential for paraxial mesoderm cell maturation and movement and repression of neural fate through repression of Wnt3a

Initiation of *Msgn1* expression in the mesoderm occurs at the late bud stage, following the activation of *Wnt3a* and *Tbx6. Msgn1* expression is reduced in *Tbx6* mutants and absent in the *Wnt3a* single and *Wnt3a*$^{-/-}$*; Tbx6*$^{-/-}$ double mutants, thereby placing Msgn1 downstream of Wnt3a and Tbx6 in the cascade, as suggested previously (Chalamalasetty et al., 2011; Wittler et al., 2007). However, upregulation and ectopic expression of *Wnt3a* in single *Msgn1*$^{-/-}$ and *Msgn1*$^{-/-}$*; Tbx6*$^{-/-}$ double mutants reveals a negative feedback loop operating on *Wnt3a*, which likely functions to restrict the activity of Wnt3a within the primitive streak. Thus, we suggest that as cells move away from the site of ingression and enter into the mesodermal cell layer, reinforcement of their commitment to paraxial mesoderm must require repression of neural markers. Indeed, this could be achieved through a synergistic action with Tbx6. Evidence for Msgn1 promoting cell migration comes from previous studies (Yoon and Wold, 2000) and from the presence of cell clusters exhibiting a neural identity located adjacent to the axial neural tube in both *Wnt3a*$^{-/-}$*; Msgn1*$^{-/-}$ and *Msgn1*$^{-/-}$*; Tbx6*$^{-/-}$ double mutants in this study. However, when compared to the organized ectopic neural tubes observed in *Tbx6*$^{-/-}$ and *Wnt3a*$^{-/-}$ mutants, only random clusters of cells were present in *Msgn1*$^{-/-}$ mutants. Since these clusters were not observed in the single *Msgn1*$^{-/-}$ mutant, this may suggest a requirement for cofactors from the signaling pathways including Wnt3a and/or Tbx6 act in, or even Tbx6 itself to initiate cell migration. Taken together the complete loss of paraxial mesoderm observed in *Msgn1*$^{-/-}$ mutants, as compared to *Wnt3a*$^{-/-}$ and *Tbx6*$^{-/-}$ mutants, supports a role for Msgn1 in facilitating the migration of cells out of the primitive streak/tail bud. Moreover, the apparent inability of cells to migrate away from their origin, as well as their failure to adopt either a paraxial mesodermal or neural fate (as confirmed by down-regulation of Sox2), may leave these cells within the tail bud in a state of indeterminacy, eventually leading to their death within the tail bud of *Msgn1*$^{-/-}$*; Tbx6*$^{-/-}$ mutants (Figure 8).

A working model for the gene regulatory network controlling paraxial mesoderm cell fate specification in the mouse

Previous studies have identified a signaling factor Wnt3a, and two transcription factors, Msgn1 and Tbx6, as the three key factors operating in the gene regulatory network regulating the paraxial mesoderm. In this study we have carried out the first comprehensive genetic study of these factors. We have performed a comparative analysis of mutants lacking each of these factors singly and in combination. Our in depth analyses have elucidated some of the unique functions of these three key factors, as well as their reciprocal interactions. Collectively, our data support a role for Wnt3a acting upstream of the two transcription factors, Tbx6 and Msgn1, in the paraxial mesoderm gene regulatory network. However, this network is not simple and unidirectional, but instead is fine-tuned by several feedback loops operating between these three key players. Furthermore, each one of these factors is likely to act in additional regulatory pathways, including with the pan-mesodermal marker *T*, necessary to establish correct and sufficient specification of paraxial mesoderm.

Conclusions

In sum, our data suggest that in epiblast cells, Wnt3a is important for EMT and cell ingression through the primitive streak, as well as for promoting neural fate by regulation of Sox2 expression during posterior somite formation. Tbx6 acts in the mesoderm where it has a dual function. It promotes differentiation of cells into paraxial mesoderm, and it suppresses neural cell fate specification by repressing *Sox2*. These conclusions are supported by a recent study (Takemoto et al., 2011). Likewise, Msgn1 also exerts at least two functions in the mesoderm where it promotes differentiation into paraxial mesoderm, and is likely a key player in regulating cell migration. In addition, both Msgn1 and Tbx6 are essential for the specification of early presomitic mesoderm that will give rise to the anterior somites. Based on current models, the Fgf signaling pathway is a plausible candidate for mediating this early phase of presomitic mesoderm specification. Future studies will be required to resolve these details and further our understanding of the mechanisms directing the formation of the paraxial mesoderm in mice, and unravel the complexities of the underlying gene regulatory networks.

Supplementary Material

Refer to Web version on PubMed Central for supplementary material.

Acknowledgments

We thank Jeong K. Yoon for the *Msgn1* mutant strain of mice and Stephanie Häusler for technical assistance. This work was supported by National Institutes of Health grants RO1-HD052115 (to A.-K.H.) and RO1-HD056248 (to V.E.P.). S.N. was supported by a fellowship from the American Heart Association (0826074) and a Development Grant from the Muscular Dystrophy Organization (186552). D.C. was supported by a National Institute of Health Ruth L. Kirschstein National predoctoral fellowship (F31 HD065441-02).

References

Cambray N, Wilson V. Axial progenitors with extensive potency are localised to the mouse chordoneural hinge. Development. 2002; 129:4855–66. [PubMed: 12361976]

Candia AF, et al. Mox-1 and Mox-2 define a novel homeobox gene subfamily and are differentially expressed during early mesodermal patterning in mouse embryos. Development. 1992; 116:1123–36. [PubMed: 1363541]

Chalamalasetty RB, et al. The Wnt3a/beta-catenin target gene Mesogenin1 controls the segmentation clock by activating a Notch signalling program. Nat Commun. 2011; 2:390. [PubMed: 21750544]

Chapman DL, et al. Tbx6, a mouse T-Box gene implicated in paraxial mesoderm formation at gastrulation. Dev Biol. 1996; 180:534–42. [PubMed: 8954725]

Chapman DL, et al. Critical role for Tbx6 in mesoderm specification in the mouse embryo. Mech Dev. 2003; 120:837–47. [PubMed: 12915233]

Chapman DL, Papaioannou VE. Three neural tubes in mouse embryos with mutations in the T-box gene Tbx6. Nature. 1998; 391:695–7. [PubMed: 9490412]

Dubrulle J, Pourquie O. Coupling segmentation to axis formation. Development. 2004; 131:5783–93. [PubMed: 15539483]

Ferrer-Vaquer A, et al. Transitions between epithelial and mesenchymal states and the morphogenesis of the early mouse embryo. Cell Adh Migr. 2010; 4

Garcia-Garcia MJ, et al. Analysis of mouse embryonic patterning and morphogenesis by forward genetics. Proc Natl Acad Sci U S A. 2005; 102:5913–9. [PubMed: 15755804]

Gont LK, et al. Tail formation as a continuation of gastrulation: the multiple cell populations of the Xenopus tailbud derive from the late blastopore lip. Development. 1993; 119:991–1004. [PubMed: 7916680]

Hadjantonakis AK, et al. Tbx6 regulates left/right patterning in mouse embryos through effects on nodal cilia and perinodal signaling. PLoS One. 2008; 3:e2511. [PubMed: 18575602]

Hofmann M, et al. WNT signaling, in synergy with T/TBX6, controls Notch signaling by regulating Dll1 expression in the presomitic mesoderm of mouse embryos. Genes Dev. 2004; 18:2712–7. [PubMed: 15545628]

Hrabe de Angelis M, et al. Maintenance of somite borders in mice requires the Delta homologue DII1. Nature. 1997; 386:717–21. [PubMed: 9109488]

Kinder SJ, et al. The orderly allocation of mesodermal cells to the extraembryonic structures and the anteroposterior axis during gastrulation of the mouse embryo. Development. 1999; 126:4691–701. [PubMed: 10518487]

Kwon GS, et al. The endoderm of the mouse embryo arises by dynamic widespread intercalation of embryonic and extraembryonic lineages. Dev Cell. 2008; 15:509–20. [PubMed: 18854136]

Naiche LA, et al. FGF4 and FGF8 comprise the wavefront activity that controls somitogenesis. Proc Natl Acad Sci U S A. 2011; 108:4018–23. [PubMed: 21368122]

Nowotschin S, et al. Dual transgene strategy for live visualization of chromatin and plasma membrane dynamics in murine embryonic stem cells and embryonic tissues. Genesis. 2009; 47:330–6. [PubMed: 19358158]

Nowotschin S, Hadjantonakis AK. Cellular dynamics in the early mouse embryo: from axis formation to gastrulation. Curr Opin Genet Dev. 2010; 20:420–7. [PubMed: 20566281]

Parr BA, et al. Mouse Wnt genes exhibit discrete domains of expression in the early embryonic CNS and limb buds. Development. 1993; 119:247–61. [PubMed: 8275860]

Pourquie O. Vertebrate somitogenesis. Annu Rev Cell Dev Biol. 2001; 17:311–50. [PubMed: 11687492]

Takada S, et al. Wnt-3a regulates somite and tailbud formation in the mouse embryo. Genes Dev. 1994; 8:174–89. [PubMed: 8299937]

Takemoto T, et al. Tbx6-dependent Sox2 regulation determines neural or mesodermal fate in axial stem cells. Nature. 2011; 470:394–8. [PubMed: 21331042]

Tzouanacou E, et al. Redefining the progression of lineage segregations during mammalian embryogenesis by clonal analysis. Dev Cell. 2009; 17:365–76. [PubMed: 19758561]

Uchikawa M, et al. Functional analysis of chicken Sox2 enhancers highlights an array of diverse regulatory elements that are conserved in mammals. Dev Cell. 2003; 4:509–19. [PubMed: 12689590]

Wilson V, et al. Stem cells, signals and vertebrate body axis extension. Development. 2009; 136:1591–604. [PubMed: 19395637]

Wittler L, et al. Expression of Msgn1 in the presomitic mesoderm is controlled by synergism of WNT signalling and Tbx6. EMBO Rep. 2007; 8:784–9. [PubMed: 17668009]

Yamaguchi TP, et al. T (Brachyury) is a direct target of Wnt3a during paraxial mesoderm specification. Genes Dev. 1999; 13:3185–90. [PubMed: 10617567]

Yoon JK, et al. The bHLH class protein pMesogenin1 can specify paraxial mesoderm phenotypes. Dev Biol. 2000; 222:376–91. [PubMed: 10837126]

Yoon JK, Wold B. The bHLH regulator pMesogenin1 is required for maturation and segmentation of paraxial mesoderm. Genes Dev. 2000; 14:3204–14. [PubMed: 11124811]

Yoshikawa Y, et al. Evidence that absence of Wnt-3a signaling promotes neuralization instead of paraxial mesoderm development in the mouse. Dev Biol. 1997; 183:234–42. [PubMed: 9126297]

Highlights

- *Wnt3a, Msgn1* and *Tbx6* mutants are characterized by the absence of paraxial mesoderm.
- Wnt3a, Msgn1 and Tbx6 are critical for paraxial mesoderm lineage commitment and differentiation in mice.
- Paraxial mesoderm progenitors are bipotential and can adopt a neural or mesodermal fate.

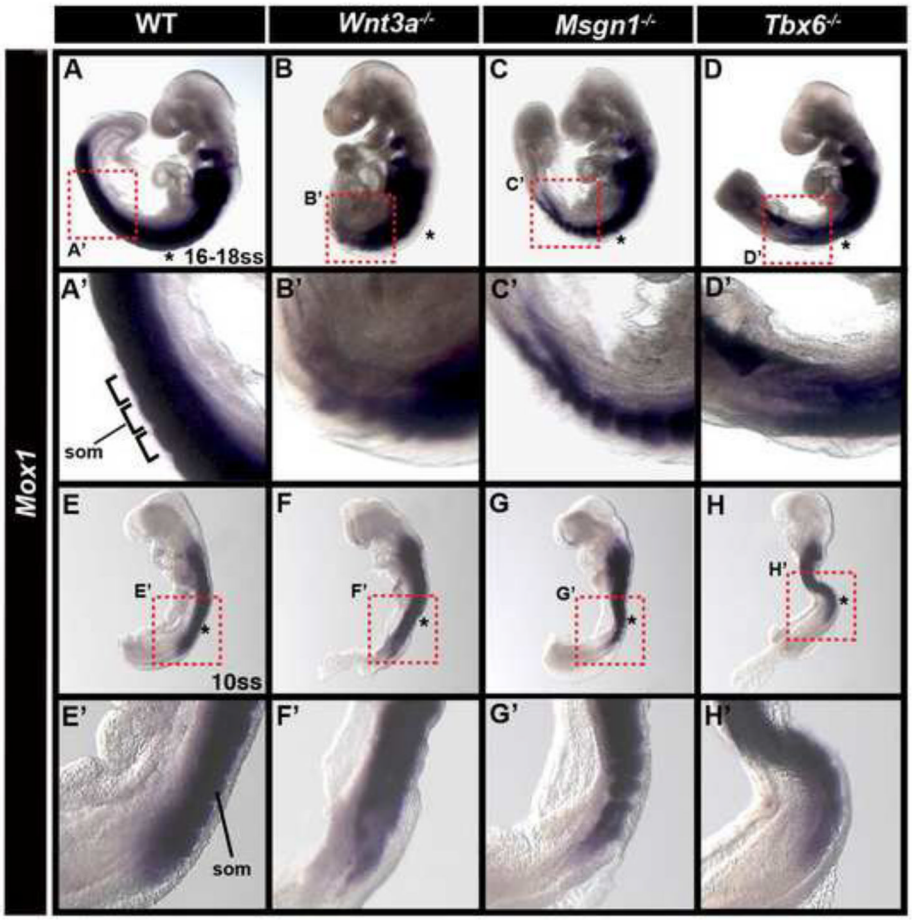

Figure 1. *Wnt3a*$^{-/-}$, *Msgn1*$^{-/-}$ and *Tbx6*$^{-/-}$ exhibit a profound loss of paraxial mesoderm and the posterior somites

Expression analysis of the paraxial mesoderm marker *Mox1* in wild-type (A, E) *Wnt3a*$^{-/-}$ (B, F), *Msgn1*$^{-/-}$ (C, G) and *Tbx6*$^{-/-}$ embryos (D, H) at 16–18ss (A–D) and 10ss (E–H) reveals lack of posterior somites in mutants. Higher magnification of the boxed areas in A–H show posterior somite region (A′–H′). Asterisks indicate position of somite 7, considered the last anterior somite. Brackets indicate one somite. som, somite; ss, somite stage.

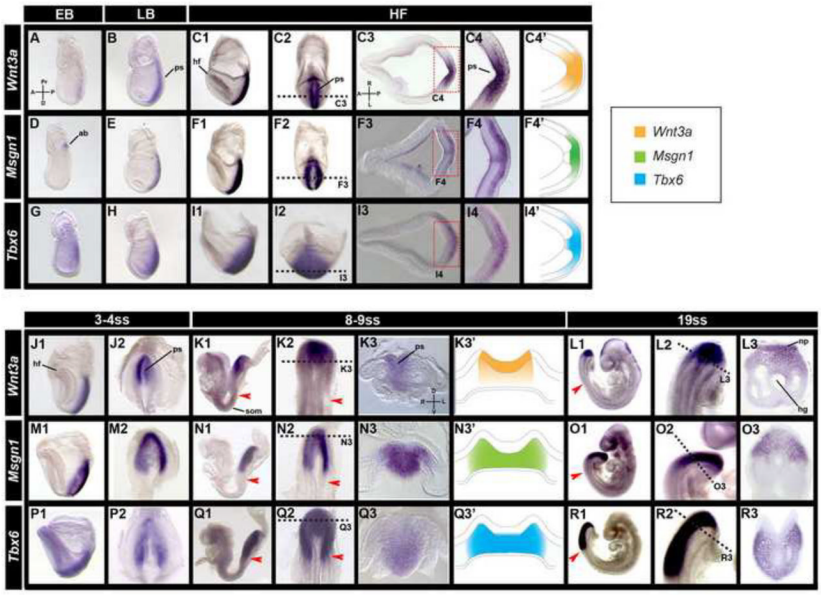

Figure 2. Expression analysis of *Wnt3a*, *Msgn1* and *Tbx6* in wild-type embryos

Dynamic expression patterns of *Wnt3a* (A–C, J–L), *Msgn1* (D–F, M–O) and *Tbx6* (G–I, P–R) at early bud (EB) (A, D, G), late bud (LB) (B, E, H), headfold stage (HF) (C, F, I), 3–4ss (J, M, P), 8–9ss (K, N, Q) and 19ss (L, O, R). Lateral views of embryo (A, B, C1, D, E, F1, G, H, I1, J1, K1, L1, M1, N1, O1, P1, Q1 and R1). Ventral views (J2, M2, P2). Posterior views (C2, F2, I2) of embryos in C1, F1 and I1, showing expression of *Wnt3a*, *Msgn1* and *Tbx6* in the primitive streak (ps) and in the presomitic mesoderm region. Transverse sections (C3, F3, I3) through HF stage embryos showing *Wnt3a* expression in the epiblast (C3) and *Msgn1* (F3) and *Tbx6* (I3) expression in the presomitic mesoderm. Higher magnifications of dashed boxes in C3, F3 and I3 (C4, F4 and I4). Schematic representations of *Wnt3a*, *Msgn1* and *Tbx6* expression at the HF stage (C4′, F4′ and I4′). Dorsal views (K2, N2, Q2) of tail region of early somite stage embryos in K1, N1 and Q1 show expression of *Wnt3a* in the primitive streak region. Expression of *Msgn1* and *Tbx6* extends anterior into the presomitic mesoderm. Transverse sections through tail region of 8–9ss embryos (K3, N3 and Q3). Schematic representations of *Wnt3a*, *Msgn1* and *Tbx6* expression at the early somite stage (K3′, N3′ and Q3′). Higher magnifications of tail region of 19ss embryos show *Wnt3a* expression restricted to the most posterior part of the tail region and more anteriorly expanded expression of *Msgn1* and *Tbx6* (L2, O2 and R2). Transverse sections through tail regions shown in L2, O2 and R2 (L3, O3 and R3). Dashed lines indicate the plane of section. Red arrows mark the boundary between presomitic mesoderm and the segmented somites (som). ab, allantoic bud; hf, head fold; hg, hind gut; np, neural plate.

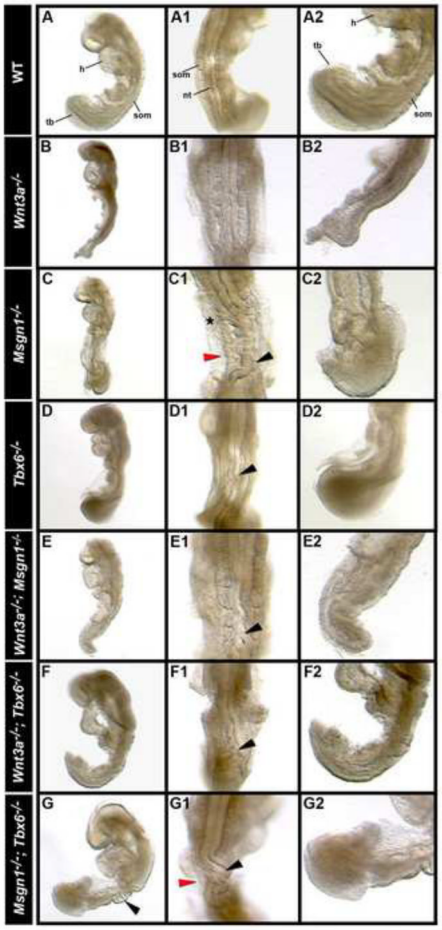

Figure 3. Gross morphology of single and double *Wnt3a*$^{-/-}$, *Msgn1*$^{-/-}$ and *Tbx6*$^{-/-}$ mutants

Morphology of a wild-type embryo showing a normal formed neural tube and properly segmented somites (som) (A). *Wnt3a*$^{-/-}$ showing loss of posterior somites (B1) and a reduced tail region (B2). *Msgn1*$^{-/-}$ (C) showing a kinked neural tube (nt), (black arrowhead), lack of paraxial mesoderm (red arrowhead) (C1) and an expanded tail region (C2). Asterisk marks a bleb resulting from defects in the vasculature of the mutant (C1). *Tbx6*$^{-/-}$ lacking posterior somites, showing aberrant anterior somites, a slightly kinked nt (black arrowhead) (D1) and an expanded tail region (D2). *Wnt3a*$^{-/-}$*; Msgn1*$^{-/-}$ double mutants (E) with loss of posterior somites (E1) and a reduced tail region (E2). *Wnt3a*$^{-/-}$*; Tbx6*$^{-/-}$ (F) displaying severely kinked nt (black arrowhead) as well as a greater reduction in mesoderm tissue (F1). *Msgn1*$^{-/-}$*; Tbx6*$^{-/-}$ (G) exhibit a severely kinked nt (black arrowhead), loss of posterior somites, severely aberrant anterior somites, loss of paraxial mesoderm (red arrowhead) (G1) and expanded tail region (G2). Lateral views of embryos (A–G). Dorsal view of embryos (A1-G1). Higher magnification of tail region (A2-G2).

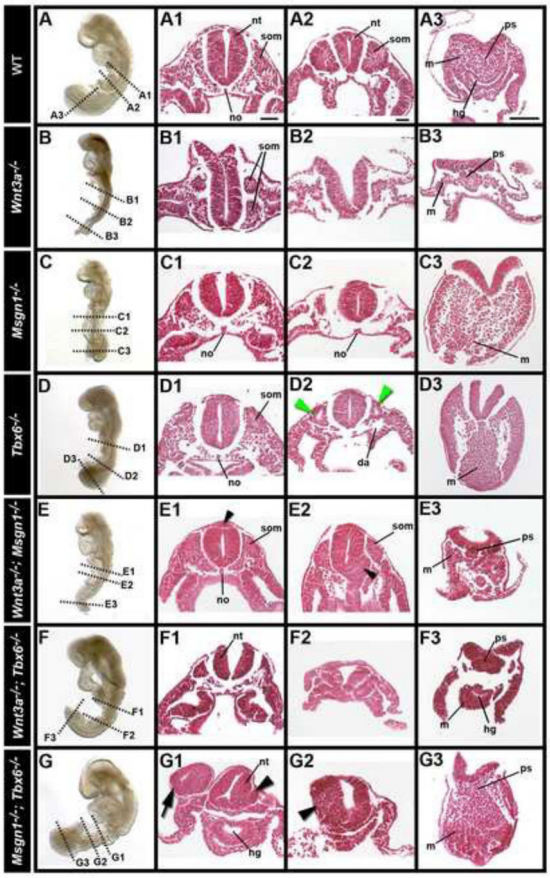

Figure 4. Histological analysis of single and double *Wnt3a*$^{-/-}$, *Msgn1*$^{-/-}$ and *Tbx6*$^{-/-}$ mutants

Whole mount and indicated transverse sections (A–G) through somite and tail regions in an anterior to posterior sequence of 12–14ss wild-type embryo (A), *Wnt3a*$^{-/-}$ (B), *Msgn1*$^{-/-}$ (C), *Tbx6*$^{-/-}$ (D), *Wnt3a*$^{-/-}$*; Msgn1*$^{-/-}$ (E), *Wnt3a*$^{-/-}$*; Tbx6* $^{-/-}$ (F) and *Msgn1*$^{-/-}$*; Tbx6*$^{-/-}$ (G). Sections show major hallmarks of the phenotype of single and double mutants: *Wnt3a*$^{-/-}$ (B) normal anterior somites (B1), loss of posterior somites (B2) and reduced tail region (B3); *Msgn1*$^{-/-}$ (C) normal anterior somites (C1), lack of posterior somites, reduced paraxial mesoderm (C2) and massively expanded tail region (C3); *Tbx6*$^{-/-}$ (D) normal anterior somites (D1), lack of posterior somites, formation of lateral ectopic neural tubes (green arrowheads) (D2) and expanded tail region (D3); *Wnt3a*$^{-/-}$*; Msgn1*$^{-/-}$ (E) normal anterior somites, cell cluster on top of the neural tube (E1) as well as ventral to neural tube (black arrowheads) (E2) and reduced tail region (E3); *Wnt3a*$^{-/-}$*; Tbx6*$^{-/-}$ (F) aberrant anterior (F1) and loss of posterior somites (F2) and reduced tail region(F3); *Msgn1*$^{-/-}$*; Tbx6*$^{-/-}$ (G) severely kinked neural tube (black arrow) (G1), cell cluster lateral to neural tube (black arrowheads) (G1 and G2), loss of posterior somites and paraxial mesoderm (G2), and expanded tail region (G3). da, dorsal aorta; hg, hindgut; m, mesoderm; no, notochord; nt, neural tube; ps, primitive streak; som, somites. Scale bar in A1 and A2: 50 μm. Scale bar in A3: 100 μm

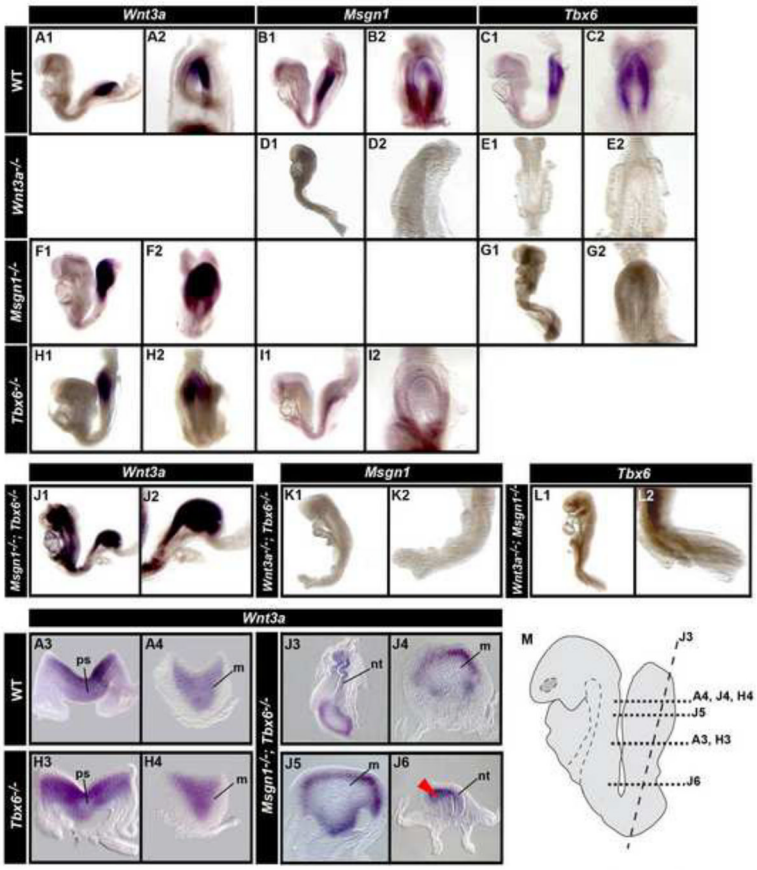

Figure 5. Expression of *Wnt3a, Msgn1* and *Tbx6* in single and double mutants during posterior somite formation

Expression patterns of *Wnt3a* (A, F, H, and J), *Msgn1* (B, D, I, and K) and *Tbx6* (C, E, G and L), respectively, in wild-type (A–C), $Wnt3a^{-/-}$ (D–E), $Msgn1^{-/-}$ (F–G), $Tbx6^{-/-}$ (H–I) $Wnt3a^{-/-}; Msgn1^{-/-}$ (L), $Wnt3a^{-/-}; Tbx6^{-/-}$ (K) and $Msgn1^{-/-}; Tbx6^{-/-}$ (J) mutants showing downregulation of *Msgn1* and *Tbx6* in $Wnt3a^{-/-}$ (D and E), upregulation of *Wnt3a* and loss of *Tbx6* in $Msgn1^{-/-}$ (F and G), upregulation of *Wnt3a* and downregulation of *Msgn1* in $Tbx6^{-/-}$ (H and I), loss of *Tbx6* expression in $Wnt3a^{-/-}; Msgn1^{-/-}$ (L), loss of *Msgn1* in $Wnt3a^{-/-}; Tbx6^{-/-}$ (K) and upregulation of *Wnt3a* in $Msgn1^{-/-}; Tbx6^{-/-}$ (J). Lateral views of whole mount embryos (A1-L1). Higher magnifications of tail region of embryos (A2-L2). Frontal section of a $Msgn1^{-/-}; Tbx6^{-/-}$ double mutant embryo showing overexpression of *Wnt3a* in the neural tube (nt) (J3). Transverse sections through $Tbx6^{-/-}$ (H3-H4) and $Msgn1^{-/-}; Tbx6^{-/-}$ (J4-J6) showing upregulation of *Wnt3a* expression in areas of the expanded tail region as well as in cell accumulations close to the neural tube (nt) of $Msgn1^{-/-}; Tbx6^{-/-}$ (J6) (red arrowhead). By comparison, transverse sections of *Wnt3a* expression in the wild-type (A3-A4). Cartoon of a 10–12ss embryo showing approximate planes of sections depicted in A3-A4, H3-H4, J3-J6 (M).

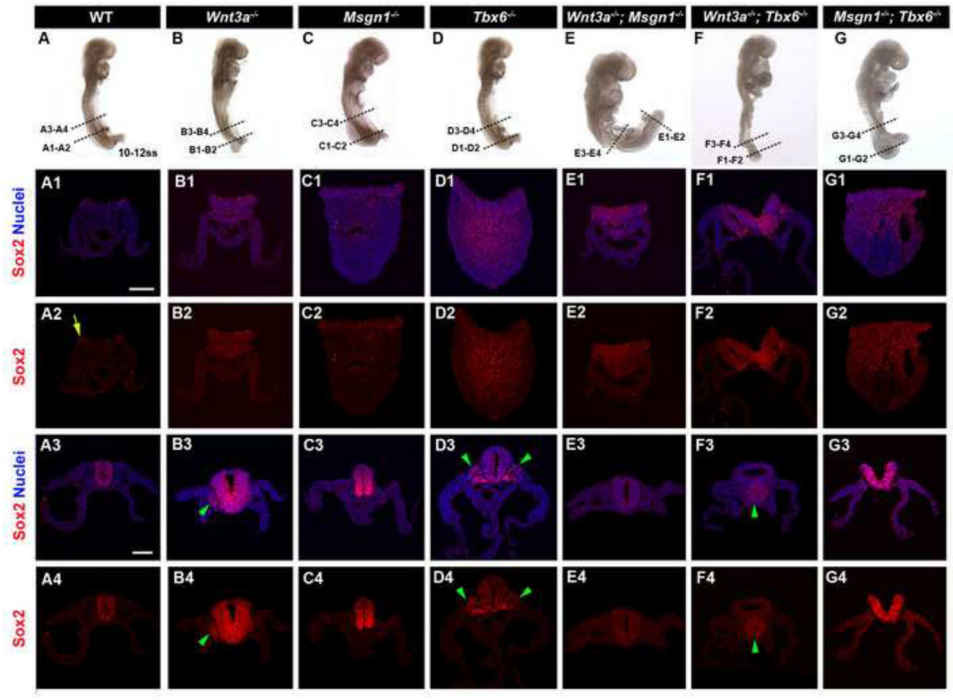

Figure 6. Upregulation of Sox2 in the tail region of 12ss *Tbx6*$^{-/-}$ and *Msgn1*$^{-/-}$; *Tbx6*$^{-/-}$ mutant embryos

Whole mount views of 10–12 somite stage (ss) wild-type (A), *Wnt3a*$^{-/-}$ (B), *Msgn1* $^{-/-}$ (C), *Tbx6*$^{-/-}$ (D) *Wnt3a*$^{-/-}$; *Msgn1*$^{-/-}$ (E), *Wnt3a*$^{-/-}$; *Tbx6*$^{-/-}$ (F) and *Msgn1*$^{-/-}$; *Tbx6*$^{-/-}$ (G) embryos. Dashed lines indicate plane of sections taken. Transverse sections through primitive streak/tail region, stained for Sox2 and Hoechst (A1-G1) and Sox2 (A2-G2). Transverse sections through region of posterior somites stained with Sox2 and Hoechst to label nuclei (A3-G3) and Sox2 (A4-G4). Green arrowheads point to ectopic neural tubes. Yellow arrow highlights Sox2 expression in the epiblast in the wild-type (A2). Scale bars in A1 and A3: 100 μm.

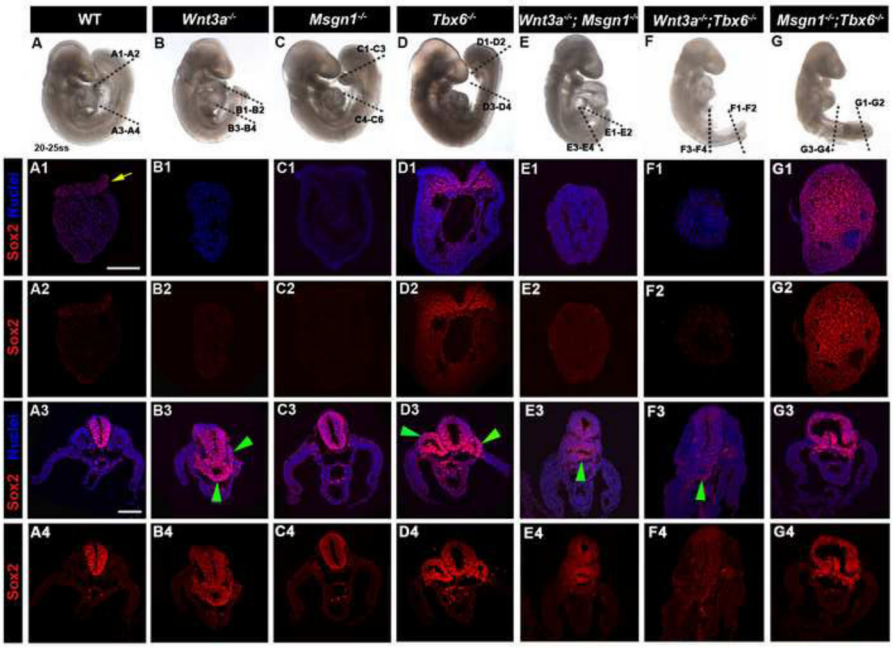

Figure 7. Upregulation of Sox2 in later stage *Tbx6*$^{-/-}$ and *Msgn1*$^{-/-}$; *Tbx6*$^{-/-}$ mutant embryos

Whole mount views of 20–25 ss wild-type (A), *Wnt3a*$^{-/-}$ (B), *Msgn1*$^{-/-}$ (C), *Tbx6*$^{-/-}$ (D), *Wnt3a*$^{-/-}$; *Msgn1*$^{-/-}$ (E), *Wnt3a*$^{-/-}$; *Tbx6*$^{-/-}$ (F) and *Msgn1*$^{-/-}$; *Tbx6*$^{-/-}$ (G) embryos. Dashed lines indicate plane of sections taken. Transverse sections through tail bud region of the embryo with immunofluorescent staining for Sox2 protein and Hoechst to label nuclei (A1-G1) and Sox2 (A2-G2). Transverse sections through region of posterior somites stained with Sox2 and Hoechst to label nuclei (A3-G3) and Sox2 (A4-G4). Green arrowheads point to ectopic (lateral and ventral) neural tubes. Yellow arrow in A1 highlights Sox2 expression in the epiblast of the wild-type. Scale bars in A1 and A3: 100 μm.

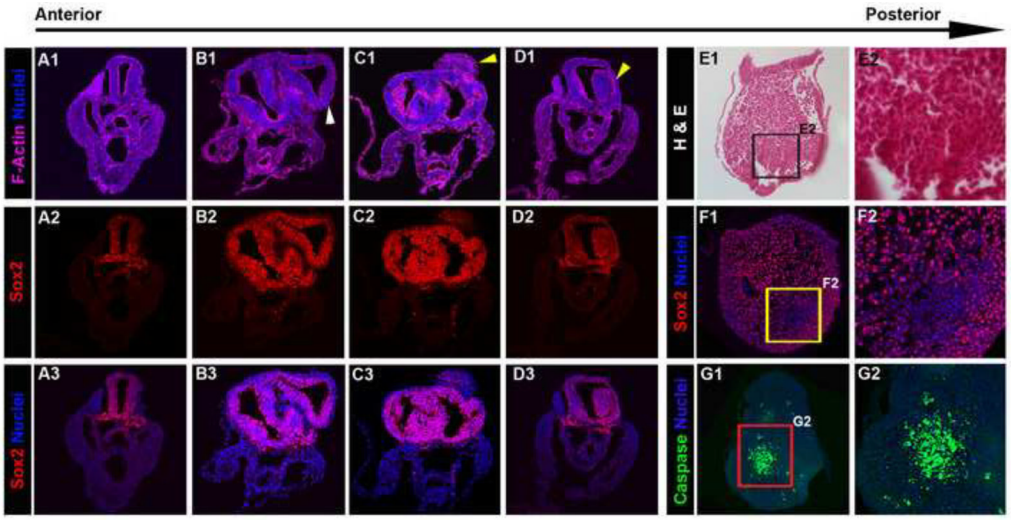

Figure 8. Ectopic neuralization and apoptosis in tail buds of *Msgn1*$^{-/-}$; *Tbx6*$^{-/-}$ mutants

Transverse sections of a 20ss *Msgn1*$^{-/-}$; *Tbx6* $^{-/-}$ embryo in anterior to posterior sequence stained with Phalloidin to label F-Actin and Hoechst to label nuclei (A1-D1), Sox2 (A2-D2), and Sox2 and Hoechst (A3-D3). Sox2 is expressed in the neural tube as well as ectopically expressed in cells enclosed within, or on top of, the neural tube (yellow arrowheads). Transverse sections through the tail bud of a 20ss *Msgn1*$^{-/-}$; *Tbx6*$^{-/-}$ embryo reveal death of cells that have downregulated Sox2. H&E stained sections (E1) and higher magnification of boxed area in E1 (E2) showing cell debris. Tail bud stained for Sox2 and Hoechst labeling nuclei (F) and immunodetection of activated Caspase (G) counterstained with Hoechst, reveal cells that undergo apoptosis have lower levels of Sox2 expression. F2 and G2 are higher magnifications of boxed areas in F1 and G1.

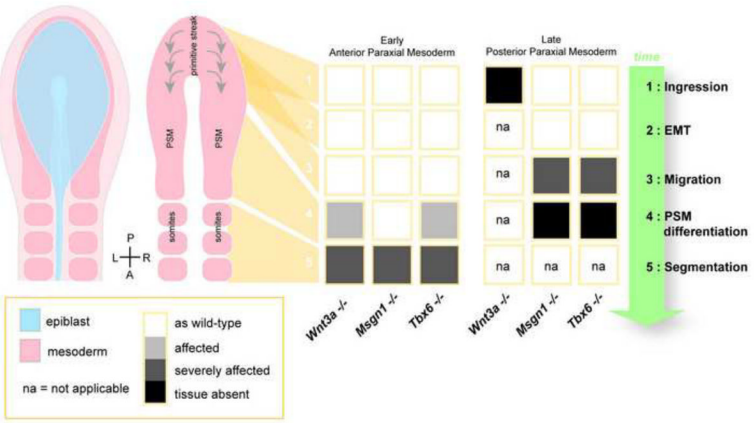

Figure 9. Summary of sequential steps in paraxial mesoderm specification and morphogenesis affected in mutants

Schematic representation depicting the sequential steps necessary for proper paraxial mesoderm specification and morphogenesis in wild-type embryos, and details of which are affected in *Wnt3a*$^{-/-}$, *Msgn1*$^{-/-}$ and *Tbx6*$^{-/-}$ mutants, respectively.

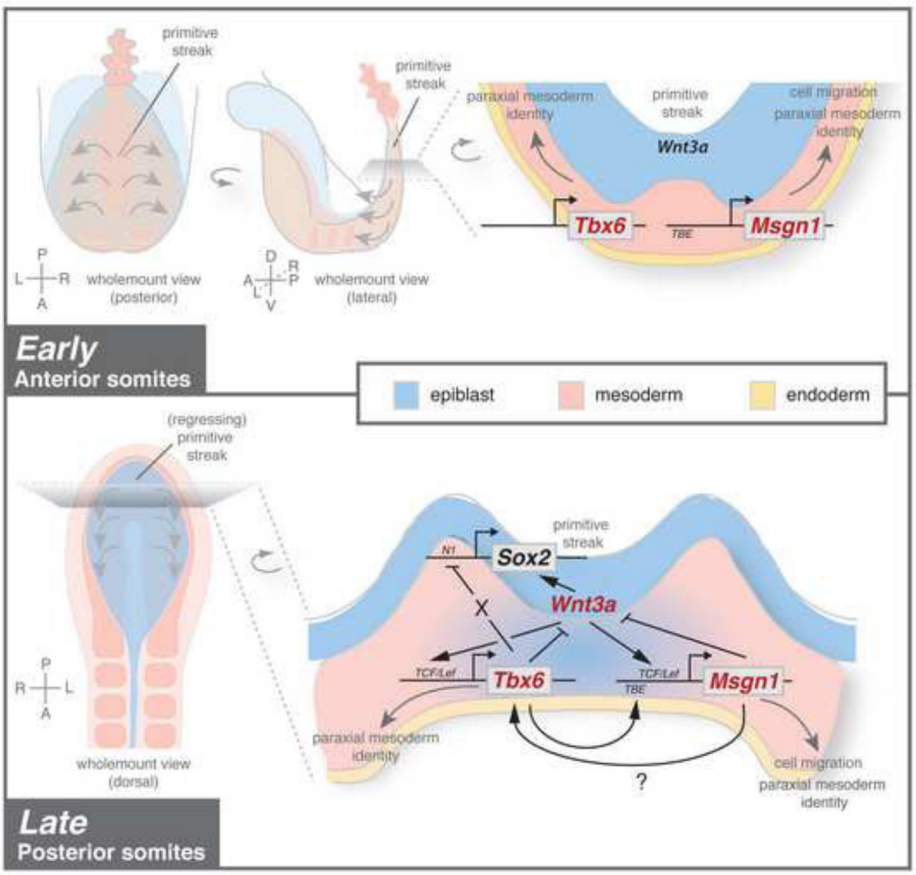

Figure 10. Working model for paraxial mesoderm specification and differentiation in the mouse embryo

Schematic representation with details of the genetic regulatory network of three critical factors, Wnt3a, Msgn1 and Tbx6, controlling paraxial mesoderm specification. This working model suggests a complex network in which Wnt3a functions at the top of the hierarchy inducing several processes that involve the activation of Tbx6 and Msgn1, several feedback loops and the involvement of each factor in possible parallel pathways for the proper specification of neural ectoderm and paraxial mesoderm, during posterior somite formation. Anterior somite formation is independent of Wnt3a function. This model focuses on paraxial mesoderm and therefore, for simplicity, does not include factors such as T/Brachyury. TBE, T-Box binding element.

Table 1

Summary of defects in single and double mutant embryos.

Genotype	Phenotypes											
	TB	**SOM**			**PSM**	**NT**	**EcNT**	**N**	**New pheno-type**	**Sox2 expression**		
		1–7	**8–11**	**post.**						**NT**	**EPI**	**TB**
Wild-type	norm	norm	norm	norm	norm	norm	none	present	na	yes	epi of ps	no
***Wnt3a*−/−**	small	norm-small	small	none	reduced	kinky	ventral, attached	absent in post	na	yes (EcNT, NT)	reduced	no
***Msgn1*−/−**	large	norm	small	none	severely reduced	very kinky	none	present	na	yes	early but not later	no
***Tbx6*−/−**	large	abnorm	none	none	reduced	kinky	lateral, not attached	present	na	yes (EcNT, NT)	yes	yes
***Wnt3a*−/−; *Msgn1*−/−**	intermed	norm-small	small	none	reduced	intermed	ventral attached	absent in post	cell cluster	low in EcNT, NT	early but not later	no
***Wnt3a*−/−; *Tbx6*−/−**	small	small abnorm	none	none	reduced	very kinky	ventral attached	absent in post	no	low in EcNT, NT	early but not later	no
***Msgn1*−/−; *Tbx6*−/−**	large	norm-small	none	none	severely reduced	very kinky	lateral, not attached	present	cell cluster	yes (EcNT, NT)	yes	yes

Abbreviations: EcNT, ectopic neural tube; epi, epiblast; intermed, intermediate; N, notochord; na, not applicable; norm, normal; NT, neural tube; PSM, paraxial mesoderm, post, posterior; ps, primitive streak; red, reduced; TB, tail bud; SOM, somites; wt, wild-type.